

Spontaneous Vortex Lattices in Quasi 2D Dipolar Spinor Condensates

Jian Zhang · Tin-Lun Ho

Received: 5 April 2010 / Accepted: 21 July 2010 / Published online: 11 August 2010
© Springer Science+Business Media, LLC 2010

Abstract Motivated by recent experiments (Vengalattore et al. in Phys. Rev. Lett. 100: 170403, 2008; Vengalattore et al., arXiv:0901.3800), we study quasi 2D ferromagnetic condensates with various aspect ratios. We find that in zero magnetic field, dipolar energy generates a local energy minimum with all the spins lie in the 2D plane forming a row of *circular* spin textures with *alternating* orientation, corresponding to a packing of vortices of *identical* vorticity in different spin components. In a large magnetic field, the system can fall into a long lived dynamical state consisting of an array of elliptic and hyperbolic Mermin-Ho spin textures, while the true equilibrium is an uniaxial spin density wave with a single wave-vector along the magnetic field, and a wavelength similar to the characteristic length of the long lived vortex array state.

Keywords Spinor condensate · Dipolar interaction · Bose-Einstein Condensate · Gross Piteavskii equation

The condensates of bosons with non-zero spins, known as spinor condensate, are remarkable superfluids. In addition to broken gauge symmetry, they also have broken symmetries in spin space. The spin degrees of freedom lead to a variety ground states, which proliferates rapidly as the value of spin increases. Since different spin components can be mixed through spin rotation, there is considerable interplay between spin and gauge degrees of freedom, leading to a whole host of new macroscopic quantum phenomena.

J. Zhang · T.-L. Ho (✉)
Department of Physics, The Ohio State University, Columbus, OH 43210, USA
e-mail: jasontlho@gmail.com

J. Zhang
Institute of Advanced Study, Tsinghua University, Beijing 10086, China

The simplest spinor condensates are those for spin-1 bosons, such as the $F = 1$ hyperfine states of ^{23}Na and ^{87}Rb . The ground state of ^{23}Na is a non-magnetic “polar” condensate whereas ^{87}Rb is a ferromagnetic condensate [3–7]. In the case of ferromagnetic condensates, they possess an additional “spin-gauge” symmetry which makes non-uniform spin textures behave like vortices [8]. The system can respond to external rotation through spin deformation. Any attempt to bend the spin will also generate vorticity.

The magnetic nature of spinor condensates naturally leads to the consideration of dipolar energy, which is intrinsic to alkali atoms. Since dipole energy can generate non-uniform spin textures, it will generate vorticity. Indeed, Yi and Pu have shown that a ^{87}Rb condensate in a sufficiently flat cylindrical potential will form a circular spin texture, which is a vortex of ferromagnetic condensate with a polar core [9]. Recently, experiments at Berkeley have shown that a ^{87}Rb condensate with a helical texture can decay into a random spin textures [1]. By estimating the energy of the final state, the authors suggest that the phenomenon is caused by dipolar energy. More recently, the Berkeley group has found that a pancake like condensate of ^{87}Rb can develop a texture with periodically modulated spin-spin correlation rotating rapidly about an in-plane magnetic field [1, 2]. They suggest that this effect is also due to dipolar energy.

Dipolar effects are highly geometry dependent. In this paper, we would like to point out that some key features of quasi 2D ^{87}Rb condensate due to dipolar interactions. Much of what we discuss also apply to other ferromagnetic condensates. We shall consider an anisotropic trap with frequencies $\omega_z \gg \omega_y > \omega_x$, as in Refs. [1, 2, 10]. The condensate is then a thin anisotropic slab in the xy -plane with Thomas-Fermi radii R_x, R_y such that $R_x/R_y = (\omega_y/\omega_x) \equiv \lambda$, ($\lambda \sim 10$ In Refs. [1, 2, 10]). In our discussions, we choose the normal to the condensate slab, $\hat{\mathbf{z}}$, to be the spin quantization axis for the condensate wavefunction $\Psi^T = (\psi_1, \psi_0, \psi_{-1})$, where the superscript “ T ” stands for transpose. We shall show that:

- (1) In zero magnetic field, dipolar energy leads to a local energy minimum consisting of a row of circular spin textures with *alternating* spin orientations in the long direction x , *with all the spins in the xy-plane*. These textures are of the Yi-Pu type [9], with a polar core and a size determined by the Thomas-Fermi radius in the short direction, R_y . This state amounts to an array of vortices in *identical vorticity* in the ψ_1 component, with ψ_{-1} being its time reversed partner. We have also found an analytic expression that well approximates this state.
- (2) In a large magnetic field \mathbf{B} in the xy -plane, the spins rotate about $\hat{\mathbf{B}}$ and experience a time averaged dipolar energy. We find that this energy is very flat in spin space around a class of textures which is an array of elliptical and hyperbolic Mermin-Ho vortices. These states are not local minima. They will eventually evolve to the true minimum, which is an uniaxial spin density wave (or “stripe phase” for short) with a single wave-vector along $\hat{\mathbf{B}}$. Due to the flatness of the energy surface, the vortex lattice textures will be very long lived during dynamical evolutions.

1 Basic Structures

We first consider some spin textures relevant for later discussions. We shall write the condensate wavefunction as $\Psi_\mu(\mathbf{x}) = \sqrt{n(\mathbf{x})}\zeta_\mu(\mathbf{x})$, where $n(\mathbf{r}) = \sum_\mu |\Psi_\mu|^2$ is the density, and $\zeta^\dagger \cdot \zeta = 1$. The spin field is given by $\mathbf{S} = \Psi_\mu^* \mathbf{F}_{\mu\nu} \Psi_\nu = n(\mathbf{x}) \mathbf{m}(\mathbf{x})$ where $\mathbf{F}_{\mu\nu}$ is the spin operator, and $\mathbf{m} = \zeta_\mu^* \mathbf{F}_{\mu\nu} \zeta_\nu$. The general form of a ferromagnetic condensate is

$$\zeta^T = e^{i\gamma}(u^2, \sqrt{2}uv, v^2) \quad \text{or} \quad \frac{\sqrt{2}\psi_1}{\psi_0} = \frac{\psi_0}{\sqrt{2}\psi_{-1}} \quad (1)$$

where $u = e^{-i\alpha/2} \cos \beta/2$, $v = e^{i\alpha/2} \sin \beta/2$. The spin is $\mathbf{m} = \cos \beta \hat{\mathbf{z}} + \sin \beta (\cos \alpha \hat{\mathbf{x}} + \sin \alpha \hat{\mathbf{y}})$, and $\mathbf{m}^2 = 1$. If the spin lies in the xy -plane, then $|u| = |v| = 1/\sqrt{2}$, (or $|\psi_1|^2 : |\psi_0|^2 : |\psi_{-1}|^2 = 1 : 2 : 1$), ζ then reduces to $\zeta^T = e^{i\gamma}(e^{-i\alpha}, \sqrt{2}, e^{i\alpha})/2$. The following cases are of interest to us. (Below, (r, ϕ) are polar coordinates.)

- (i) *Elliptic planar texture*: This corresponds to $\Psi^T(x, y) = \sqrt{n}(\mp ie^{-i\phi} f(r), \sqrt{2}, \pm ie^{i\phi} f(r))$, where $f(r)$ vanishes at $r = 0$ and becomes 1 beyond a healing length ξ . This describes a ferromagnet ($\mp ie^{-i\phi}, \sqrt{2}, \pm ie^{i\phi})/2$) (at large distance) with a polar core $(0, 1, 0)$ (at $r = 0$). All spins line up in circles in the xy -plane, with a magnitude $|\mathbf{m}|$ shrinks from 1 to zero as $r \rightarrow 0$, (a “meron”). This is the state found by Yi and Pu [9]. Figures 1a and 1b show the spin textures of Ψ with upper and lower sign, which have opposite spin orientations. Note that reversing spin orientation does not alter the phase winding (or circulation) of each spin component.
- (ii) *Hyperbolic planar texture*: This is the same as (i) except with $\phi \rightarrow -\phi$. See Figs. 1c and 1d.
- (iii) *Elliptic Mermin-Ho texture* [11]: This corresponds to $\Psi^T = \sqrt{n}(\cos^2 \frac{\beta(r)}{2}, i\sqrt{2}e^{i\phi} \cos \frac{\beta(r)}{2} \sin \frac{\beta(r)}{2}, -e^{2i\phi} \sin^2 \frac{\beta(r)}{2})$ where $\beta(r)$ is an increasing function of r starting with $\beta(0) = 0$. As r increases from 0 to a distance where $\beta = \pi/2$, ζ changes from $(1, 0, 0)$ to $(1, i\sqrt{2}e^{i\phi}, -e^{2i\phi})$, which has the same circular spin

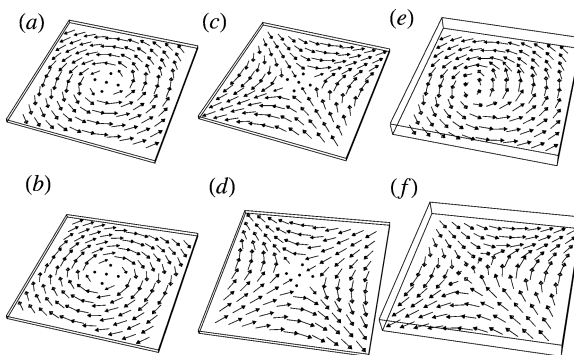


Fig. 1 (a) and (b) are elliptic planar textures with identical vorticity in ψ_1 and ψ_{-1} . (c) and (d) are hyperbolic planar spin textures with identical vorticity. All these spin textures (a)–(d) have a polar core. (e) and (f) are elliptic and hyperbolic Mermin-Ho textures. The cores are fully ferromagnetic

texture as (i) at large distance. It differs from (i) in that it is everywhere ferromagnetic. Vortex singularities can be eliminated without damaging the ferromagnetic order. See Fig. 1e.

(iv) *Hyperbolic Mermin-Ho texture*: This is the same as (iii) with $\phi \rightarrow -\phi$.

2 Energetic Considerations

We shall discuss the zero field case at zero temperature. Although $B \neq 0$ in current experiments, we first discuss this case because of its fundamental importance. In zero magnetic field, the energy is $E[\Psi] = \mathcal{T} + \mathcal{V} + \mathcal{U} + \mathcal{V}_D$, where $\mathcal{T} = \int \frac{\hbar^2}{2M} \nabla |\Psi_\mu|^2$ is the kinetic energy, $\mathcal{V} = \int V(\mathbf{x}) n(\mathbf{x})$ is harmonic trap, $V(\mathbf{x}) = \frac{1}{2} M (\omega_x^2 x^2 + \omega_y^2 y^2 + \omega_z^2 z^2)$, $\mathcal{U} = \int \frac{1}{2} [c_0 n^2 + c_2 \mathbf{S}^2]$ describes density repulsion ($c_0 > 0$) and ferromagnetic interaction ($c_2 < 0$) [3–7], $\mathcal{V}_D = \frac{1}{2} g_D \int S_i(\mathbf{x}) D_{ij}(\mathbf{x} - \mathbf{x}') S_j(\mathbf{x}')$ is the dipolar energy, where $D_{ij}(\mathbf{x}) = \delta_{ij}/x^3 - 3x_i x_j/x^5$, $g_D = \gamma^2$, $\gamma = g_F \mu_B$, $g_F = -1/2$ is the magnetic g -factor, and μ_B is the Bohr magneton. Noting that $D_{ij}(\mathbf{x}) = -\nabla_i \nabla_j \frac{1}{|\mathbf{x}|} - \frac{4\pi}{3} \delta_{ij} \delta(\mathbf{x})$, we have

$$\mathcal{V}_D = \frac{g_D}{2} \left[\int_{\mathbf{x}, \mathbf{x}'} \frac{Q(\mathbf{x}) Q(\mathbf{x}')}{|\mathbf{x} - \mathbf{x}'|} - \frac{4\pi}{3} \int_{\mathbf{x}} \mathbf{S}^2(\mathbf{x}) \right], \quad (2)$$

where $Q(\mathbf{x}) = \nabla \cdot \mathbf{S}(\mathbf{x})$. The first term in (2) is positive definite, the optimum spin configuration is the one that satisfies $\nabla \cdot \mathbf{S} = 0$ while keeping $|\mathbf{m}| = 1$ to gain maximum ferromagnetic energy. The difficulty in finding the equilibrium textures is that these two conditions are not always compatible.

For ^{87}Rb , $c_2/c_0 = 0.005$ [1], the healing length for spin is much longer than that for density, and exceeds the thickness of the “pancake” condensates. The spin degrees of freedom is effectively 2D, in the sense that

$$\Psi_\mu(x, y, z) = \sqrt{n(x, y, z)} \zeta_\mu(x, y), \quad (3)$$

and \mathbf{m} depends only on (x, y) . Since $n(\mathbf{x})$ is mirror symmetric about the xy -plane, the term QQ in (2) can be replaced by $Q_{//}(\mathbf{x})Q_{//}(\mathbf{x}') + Q_{\perp}(\mathbf{x})Q_{\perp}(\mathbf{x}')$, where $Q_{//}(\mathbf{x}) = m_z(\mathbf{x}_{\perp}) \partial_z n(\mathbf{x})$, and $Q_{\perp}(\mathbf{x}) = \nabla_{\perp} \cdot \mathbf{S}_{\perp}(\mathbf{x})$, $\nabla_{\perp} = (\nabla_x, \nabla_y)$, $\mathbf{S}_{\perp} = (S_x, S_y)$. The energy is minimized by $m_z = Q_{\perp} = 0$, or simply $\nabla_{\perp} \cdot \mathbf{S} = 0$ with \mathbf{S} in the xy -plane. In regions where density is uniform, these conditions can be satisfied by the elliptic planar texture (i) mentioned above. Indeed, circular spin alignment are prevalent in all cases we studied. Their presence, however, often require some fractions of their hyperbolic counterparts to facilitate their close packing, even though the latter are not as energetically favorable.

3 Our Calculation

For simplicity, we take the density to be a Gaussian along z and Thomas-Fermi in xy -plane, $n(x, y, z) = w(z)^2 n_{TF}(x, y)$, where $w(z) = e^{-z^2/2d^2}/(\pi^{1/4} d^{1/2})$, d is the width of the condensate along z , and $n_{TF}(\mathbf{r}) = [\mu - \frac{1}{2}(M\omega_x^2 x^2 + M\omega_y^2 y^2)]/\tilde{c}_o$,

$\tilde{c}_o = c_o/(\sqrt{2\pi}d)$, $\mathbf{r} = (x, y)$, and μ is the chemical potential determined by the total number of particles. We have ignored the effect of c_2 on the density since $c_2/c_0 = 0.005$ [1]. With this density, all the variational variables are contained in ζ . Since ζ is a three component complex vector, it is described by six real fields. The normalization of ζ reduces the number of independent real fields to five, which we denoted as $\{X_i(\mathbf{r}), i = 1, \dots, 5\}$. The energy $E[\Psi]$ is therefore a function of these five fields $E[\Psi] = E[\{X_i\}]$, and the equilibrium condition is given by $\delta E/\delta X_i = 0$.

To locate the energy minima, we use the standard numerical “relaxation” scheme to evolve the variables $X_i(\mathbf{r})$ by a fictitious dissipative dynamics $dX_i(\mathbf{r}, t)/dt = -\Gamma_i \frac{\delta E[X_j]}{\delta X_i(\mathbf{r}, t)}$, where $\Gamma_i > 0$. The evolution guarantees that $dE/dt = -\int d\mathbf{r} \sum_{i=1}^5 \Gamma_i (\delta E/\delta X_i(\mathbf{r}, t))^2 < 0$, it forces the energy to decrease, coming to a stop only when a local minimum ($\delta E/\delta X_i = 0$) is reached. Starting this evolution with different initial conditions, one can locate the energy minimum while mapping out the energy surface in the space of $\zeta(\mathbf{r})$, or $\{X_i(\mathbf{r})\}$.¹ The parameters Γ_i are chosen to ensure fast convergence. They are merely mathematical devices to enable the evolution to reach the minimum efficiently, and are not related to any physical parameters. Many phenomena are found in these evolution, from which we have reached the conclusions in the next two sections. In particular, we would like to point out that some very tricky points in this evolution. We find that the derivative $\frac{\delta E[X_j]}{\delta X_i(\mathbf{r}, t)}$ can change by six orders of magnitude during the evolution, the most rapid change corresponds to creation and disappearance of topological structures. Because of this rapid change, special adjustment of the time step has to be made in order to ensure the accuracy of the evolution. In the case of zero magnetic field, the convergence of the evolution is reasonably fast, typically takes a day on a fast laptop. In the case of large magnetic field (discussed in Sect. 5 below), one encounters some very slow evolution, it can take up to a week for the system to converge. The slow evolution indicates that the derivative $\frac{\delta E[X_j]}{\delta X_i(\mathbf{r}, t)}$ is almost vanishing, meaning that the energy surface has a very flat portion.

4 Zero Field Case

We have performed imaginary time evolution for a system with 10^6 particles for different aspect ratios λ and different initial states: random configurations, spiral spin textures, and vortex lattice textures. In all cases, the final state is either a uniform texture, or a state $\Psi^{(o)}$ with a row of circular planar texture (type (i) in Sect. 1 with alternating orientations. The texture for the $\lambda = 10$ case is shown Fig. 2. All the spins indeed lie in the xy -plane as discussed in Sect. 2.

Based on the discussions in Sect. 1, we find that our numerical result $\Psi^{(o)}$ can be described accurately by

$$\tilde{\Psi}(x, y, z)^T = \sqrt{n}(e^{i\Phi(\mathbf{r})} f(\mathbf{r}), \sqrt{2}, e^{-i\Phi(\mathbf{r})} f(\mathbf{r})) \quad (4)$$

¹We use the parameters similar to those in Refs. [1, 2]: Atom number $N \sim 3 \times 10^6$, $(\omega_x, \omega_y, \omega_z) = 2\pi(3.9, 39, 440)$ Hz, $B = 150$ mG, $c_2 n_0 = -h$ (10.7 Hz) where n_0 is the peak density, $g_D/c_2 = 0.08$. Quadratic Zeeman shift at this field is $q = h$ (1.5 Hz), or $2q/\hbar\omega_y = 0.1$. Defining the dipolar length ξ_D as $g_D n = \hbar^2/(2M\xi_D^2)$, we find $\xi_D \sim 10$ μm. We thank Dr. Vengalattore for these information.

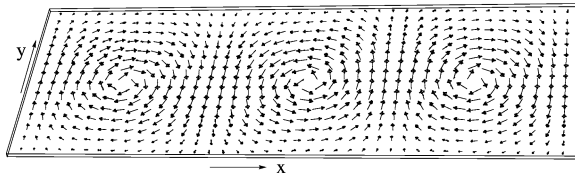


Fig. 2 The middle section of the texture of an energy minimum of a system with aspect ratio $\lambda = 10$ in zero magnetic field. The state consists of a row of elliptic planar textures with alternating spin orientations. All spins lies in the xy -plane. See Figs. 1a and 1b

where $n = w^2(z)n_{TF}(\mathbf{r})$, $\mathbf{r} = (x, y)$, $\Phi(\mathbf{r})$ is the phase angle of the 1D vortex lattice,

$$\Phi(x, y) = \pi/2 + \arg \mathcal{P}(z), \quad z = x + iy, \quad (5)$$

and $\mathcal{P}(z) = \prod_n (z - a - nb)$, $n = 0, \pm 1, \pm 2, \dots, \pm M$ is a polynomial describing an array of vortices of *identical* circulation centered at $x = a$, separated by distance b along the x axis. We find that when λ is an odd (even) integer, $a = 0$ ($a = b/2$). M is the smallest integer such that $(M+1)b > R_x$. The function f describes the vortex core with size ξ .² For all aspect ratios we examined, the optimal value of b (the size of the circular planar unit) and ξ (core size) is found to be ~ 1.5 and ~ 0.25 in units of R_y (the shorter Thomas-Fermi in the xy -plane).

The packing of vortices with identical vorticity in both $\tilde{\psi}_1$ and $\tilde{\psi}_{-1}$ may seem surprising, for it costs kinetic energy. The reason is that this is the only packing that leads to circular spin textures, which is strongly favored by dipolar energy. With dipolar energy scales as n^2 and kinetic energy scales as n , the condensate wavefunction will be determined by the former. Our calculations show that the vortex row state $\Psi^{(o)}$ is the ground state for $\lambda \leq 2$. For $\lambda > 2$, the ground state is a uniform spin texture along \hat{x} , while $\Psi^{(o)}$ is a local minimum.³

5 A Large Magnetic Field \mathbf{B}

In a magnetic field \mathbf{B} , the energy acquires linear and quadratic Zeeman shift, $\mathcal{E}_1 = -\int \gamma \mathbf{B} \cdot \Psi_\mu^* \mathbf{F}_{\mu\nu} \Psi_\nu$ and $\mathcal{E}_2 = \int q \Psi_\mu^* (\hat{\mathbf{B}} \cdot \mathbf{F})_{\mu\nu}^2 \Psi_\nu$. For sufficiently large magnetic field, the spin texture of the system will rotate about \mathbf{B} . In the frame rotating about $\hat{\mathbf{B}}$ with Lamor frequency, the linear Zeeman shift is transformed away. Dipolar

²We take $f(r) = \tanh^2(r/\xi)$. The quadratic power is due to the spin mixing term in the Gross-Pitaevskii equation. The angle $\pi/2$ in (5) is crucial for creating a circular spin texture. The opposite orientation of the neighboring circular units in see Fig. 2 is due to the change of sign of $\mathcal{P}(z)$ as one passes through a vortex from left to right.

³The energy of the vortex row state $\Psi^{(o)}$ is basically a sum of the “self” energy of individual circular spin textures. Their interaction energy can be ignored because the effective “dipole moment” of each unit is essentially zero. On the other hand, a uniform texture can be viewed as an 1D array of “giant dipoles” obtained by turning each circular spin unit in the original circular spin array into a unit uniform texture. While each of these “dipole” has higher self energy than the circular unit, they interact much strongly with each other. As λ increases, the interaction energy in the uniform spin units will outweigh the self energy of the circular units. The switch appears at $\lambda = 2$.

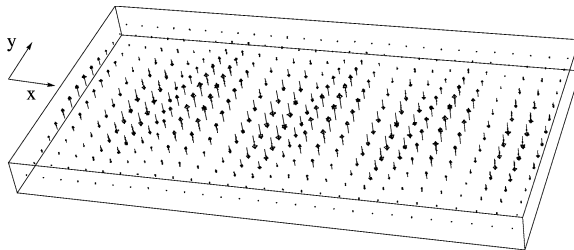


Fig. 3 The middle section of the texture of the equilibrium state of \overline{E} for a system with aspect ratio $\lambda = 10$

energy, however, acquires time dependent terms in this frame that oscillates with the Lamour frequency. Over times much longer than the Lamor cycle, the system sees an averaged dipolar energy $\overline{\mathcal{V}_D} = \int S_i(\mathbf{r}) \overline{D}_{i,j}(\mathbf{r} - \mathbf{r}') S_j(\mathbf{r}')$, where

$$\overline{D}_{i,j}(\mathbf{x}) = \frac{(3\hat{\mathbf{B}}_i\hat{\mathbf{B}}_j - \delta_{ij})}{2|\mathbf{x}|^3} \left(1 - \frac{3(\hat{\mathbf{B}} \cdot \mathbf{x})^2}{|\mathbf{x}|^2} \right). \quad (6)$$

The total time averaged energy is then $\overline{E} = \mathcal{T} + \mathcal{V} + \mathcal{U} + \overline{\mathcal{V}_D} + \mathcal{E}_2$. Note that \overline{E} conserves $\hat{\mathbf{B}} \cdot \int \mathbf{S}$. In Refs. [1, 2], $\hat{\mathbf{B}}$ is aligned with $\hat{\mathbf{x}}$ up to a few degrees. The observed state with periodic spin texture is found to have $\int S_x \sim 0$ and with most spins lie perpendicular to $\hat{\mathbf{x}}$.

To search for the stationary states of \overline{E} with $\int S_x \sim 0$, we performed the dissipative dynamics mentioned in Sect. 3 with a great variety of initial conditions. Depending on the quadratic Zeeman energy (q), two types of stationary state emerge. For $q/\hbar\omega_y > (q/\hbar\omega_y)_c \sim 0.1$, the equilibrium state is an uniaxial spin density wave with $\mathbf{S}(\mathbf{r}) = \hat{\mathbf{z}} \cos(K\hat{\mathbf{B}} \cdot \mathbf{r})$. For the parameters used in footnote 1, we find a wavelength $2\pi/K \sim 12.5a_y \sim 25 \mu\text{m}$, ($a_y = \sqrt{\hbar/(M\omega_y)}$) and is independent of the angle between $\hat{\mathbf{B}}$ and $\hat{\mathbf{x}}$. For $q/\hbar\omega_y < (q/\hbar\omega_y)_c$, the system will settle in a state consisting of two large uniform spin domains along $\hat{\mathbf{x}}$ and $-\hat{\mathbf{x}}$, with a pair of elliptic and hyperbolic Mermin-Ho textures sandwiched in between (Fig. 3).

In addition to these two equilibrium states, we also find a class of spin textures which are essentially distorted vortex lattices which remain in the imaginary time evolution for a very long time, reflecting the flatness of the energy surface in the neighborhood of these states. The underlying structure of these distorted lattice are pairs of elliptic and hyperbolic MH vortices (see Fig. 4), with essentially zero spin projection along $\hat{\mathbf{x}}$, $\int S_x/N \sim 10^{-3}$. These states remain long lived for $q/\hbar\omega_y < 0.2$ and begin to evolve more rapidly toward the stripe phase as q increases. We have calculated the spin-spin correlation function $G(\mathbf{r})$ as defined in Ref. [1] for the vortex arrays in Fig. 4. The result is shown in Fig. 5 where bright color represents a high value of $G(\mathbf{r})$. The underlying lattice structure of the disordered spin texture Fig. 4 shows up a lattice of bright spots in Fig. 5.

In Fig. 6, we have plotted $|S(\mathbf{K})|^2$, where $\mathbf{S}(\mathbf{K})$ is the Fourier transform of spin texture $\mathbf{S}(\mathbf{r})$ shown in Fig. 4. The almost periodic structure in real space shows up as intense spots in K -space. Taking the brightest spot closest to the origin on the right, we find $(a_y/\lambda_x, a_y/\lambda_y) \sim (0, 0.08)$, or $\sqrt{\lambda_x^2 + \lambda_y^2} \sim 25 \mu\text{m}$, comparable to the period

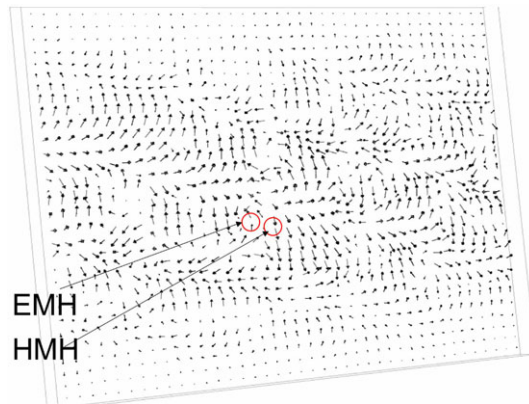


Fig. 4 (Color online) A long lived state of the time average energy \bar{E} —an array of elliptic and hyperbolic Mermin-Ho vortex pair

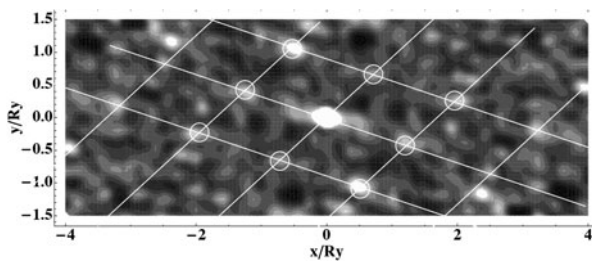


Fig. 5 Spin-spin correlation of the state in Fig. 4. Note that the bright spots form an almost square lattice

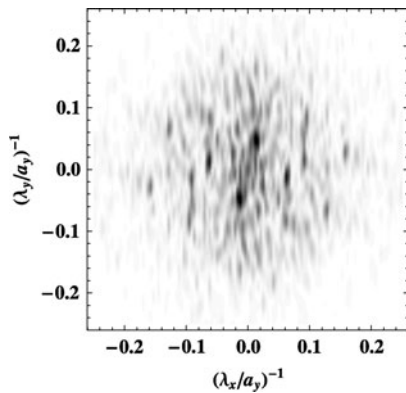


Fig. 6 $|S(\mathbf{K})|^2$ of the state in Fig. 4; $\mathbf{K} = 2\pi(\lambda_x^{-1}, \lambda_y^{-1})$

found in the stripe phase, and is the same order of the “dipolar length” (see footnote 1). We note that the corresponding plot in Ref. [1] shows a length scale $\sim 10 \mu\text{m}$, differing from our result by a factor of 2. This difference may be due to our Gaussian approximation of the actual density normal to the plane, which will contribute to systematic errors in the energies of all textures. However, such systematic error will not change the fact that both the stripe phase and the spin lattice textures have similar length scales—a property that can be verified by experiments.

Since the long lifetime in this dissipative evolution is due to the almost vanishing $\delta E/\delta\zeta$, similar long lifetime will also occur in real time evolution as it is driven by the same derivative. Our findings, which are consistent with those in Refs. [1, 2], suggest that the observed periodic structure is a long lived dynamical state. They also predict two equilibrium configurations: a row of alternating circular spin texture in zero field, and a single wavevector spin stripe phase in large magnetic field. Our method is also applicable to other dipolar condensates.

We thank Dan Stamper-Kurn and Mukund Vengalattore for discussions. This work is supported by ARO Grant W911NF0710576 for the DARPA OLE Program, and by NSF Grants PHY-05555576, DMR0705989.

References

1. M. Vengalattore et al., Phys. Rev. Lett. **100**, 170403 (2008)
2. M. Vengalattore et al., [arXiv:0901.3800](https://arxiv.org/abs/0901.3800)
3. T.L. Ho, Phys. Rev. Lett. **81**, 742 (1998)
4. J. Stenger et al., Nature **396**, 345 (1998)
5. M.-S. Chang et al., Nat. Phys. **1**, 111 (2005)
6. J. Kronjager et al., Phys. Rev. Lett. **97**, 110404 (2006)
7. L. Sadler et al., Nature **443**, 312 (2006)
8. T. Ohmi, K. Machida, J. Phys. Soc. Jpn. **67**, 1822 (1998)
9. S. Yi, H. Pu, Phys. Rev. Lett. **97**, 020401 (2006)
10. M. Vengalattore et al., Phys. Rev. Lett. **98**, 200801 (2007)
11. N.D. Mermin, Tin-Lun Ho, Phys. Rev. Lett. **36**, 594 (1976)